Nanotechnology

DOI: 10.1002/ange.201106998

$LiNi_{0.5}Mn_{1.5}O_4$ Hollow Structures as High-Performance Cathodes for Lithium-Ion Batteries

*Liang Zhou, Dongyuan Zhao, and XiongWen (David) Lou**

Lithium-ion batteries (LIBs), which are the dominant power source for portable electronics, have also gained enormous interest recently for large-scale applications, such as electric vehicles (EV), hybrid electric vehicles (HEV), and stationary energy storage.[1] To meet the requirements of these applications, further improvements in terms of energy and power densities, safety, and lifetime are required. However, conventional micrometer-sized bulk electrode materials are reaching their inherent limits in performance and unable to fully satisfy the increasing demands. Nanostructured electrode materials hold the key to overcome the limits, especially the power density.[1c,2] Taking the well-known cathode material $LiMn_2O_4$ as an example, various nanostructures, such as nanoparticles,[3] nanowires,[4] nanotubes,[5] hollow spheres,[6] and ordered mesoporous/macroporous materials,[7] have been fabricated to improve the rate capability. When compared to pristine $LiMn_2O_4$, Ni-doped $LiNi_{0.5}Mn_{1.5}O_4$ shows significantly improved cycling performance and increased energy density.[8] However, types of $LiNi_{0.5}Mn_{1.5}O_4$ nanostructures reported are rather limited, which is mainly due to undesirable particle growth during the essential high-temperature sintering process. During conventional synthesis of $LiNi_{0.5}Mn_{1.5}O_4$, the raw materials used are usually in micrometer scale and mixed by grinding or ball-milling methods. Atomic migration over micrometer scale during the subsequent high-temperature sintering process will likely lead to undesirable particle growth. Although the undesirable particle growth can be partly prevented by adding growth inhibitors, the resultant products are usually composed of irregular nano- or microparticles.[8c,d] Thus, morphologically controlled synthesis of $LiNi_{0.5}Mn_{1.5}O_4$ nanostructures remains a great challenge.

Herein, we present a morphology-controlled synthesis of $LiNi_{0.5}Mn_{1.5}O_4$ hollow microspheres and microcubes with nanosized subunits by an impregnation method followed by a simple solid-state reaction. The impregnation method provides homogeneous distribution of the reagents at nanoscale. As the distance for atomic migration is shortened significantly to several nanometers, the undesired particle growth during the annealing is effectively suppressed in the present synthesis. The resultant $LiNi_{0.5}Mn_{1.5}O_4$ hollow structures exhibit a discharge capacity of about $120\,mA\,h\,g^{-1}$, with excellent cycling stability and superior rate capability.

Figure 1 illustrates the procedure for the fabrication of $LiNi_{0.5}Mn_{1.5}O_4$ hollow structures. Uniform $MnCO_3$ microspheres and microcubes (Supporting Information, Figure S1 and S2) prepared by the precipitation method are employed as the precursors in the synthesis. In step 1, the $MnCO_3$ microspheres and microcubes are converted into MnO_2 by thermal decomposition at 400 °C according to $2MnCO_3 + O_2 \rightarrow 2MnO_2 + 2CO_2$. The microsphere/microcube morphology is retained after the annealing process (Supporting Information, Figure S3 and S4). Owing to the release of CO_2 in the thermal decomposition, the obtained MnO_2 microspheres/microcubes are highly porous. In step 2, $LiOH{\cdot}H_2O$ and $Ni(NO_3)_2{\cdot}6H_2O$ are introduced into the mesopores of the MnO_2 microspheres/microcubes by a simple impregnation method. The reactions involved in step 3 are multi-step and rather complicated. Briefly, it could involve the following processes: the dehydration of $LiOH{\cdot}H_2O$ ($LiOH{\cdot}H_2O \rightarrow LiOH + H_2O$); the decomposition of MnO_2 ($4MnO_2 \rightarrow 2Mn_2O_3 + O_2$); the decomposition of $Ni(NO_3)_2{\cdot}6H_2O$ ($2Ni(NO_3)_2{\cdot}6H_2O \rightarrow 2NiO + 4NO_2 + 12H_2O + O_2$); and finally lithiation ($8LiOH + 6Mn_2O_3 + 4NiO + 3O_2 \rightarrow 8LiNi_{0.5}Mn_{1.5}O_4 + 4H_2O$). The fusion of the mesopores and a mechanism analogous to the Kirkendall effect, that is, the fast outward diffusion of Mn and Ni atoms and the slow inward diffusion of O atoms, are proposed to be responsible for the formation of the hollow cavity in the $LiNi_{0.5}Mn_{1.5}O_4$ microspheres/microcubes.[9]

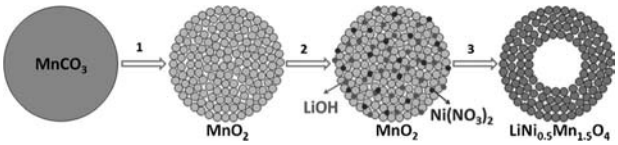

Figure 1. Illustration of the fabrication of $LiNi_{0.5}Mn_{1.5}O_4$ hollow microstructures (see text for details).

The resultant products were initially characterized by X-ray diffraction (XRD) to identify the crystallographic structure and crystallinity, and the diffraction patterns are presented in Figure 2. Both patterns can be assigned to well-crystallized cubic spinel $LiNi_{0.5}Mn_{1.5}O_4$ (JCPDS Card No.: 80-2162, space group: $Fd\bar{3}m$, $a = b = c = 8.170$ Å), with

[*] Dr. L. Zhou, Prof. X. W. Lou
School of Chemical and Biomedical Engineering
Nanyang Technological University
70 Nanyang Drive, Singapore 637457 (Singapore)
and
Energy Research Institute @ NTU, Nanyang Technological University
50 Nanyang Drive, Singapore 637553 (Singapore)
E-mail: xwlou@ntu.edu.sg
Homepage: http://www.ntu.edu.sg/home/xwlou/
Prof. D. Y. Zhao
Department of Chemistry and Shanghai Key Laboratory of Molecular Catalysis and Innovative Materials, Laboratory of Advanced Materials, Fudan University, Shanghai 200433 (P. R. China)

Supporting information for this article is available on the WWW under http://dx.doi.org/10.1002/anie.201106998.

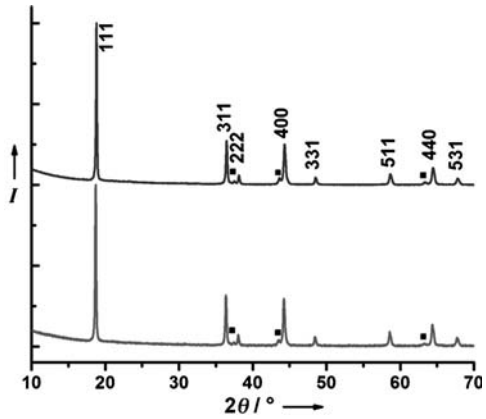

Figure 2. XRD patterns of $LiNi_{0.5}Mn_{1.5}O_4$ hollow microspheres (lower trace) and hollow microcubes (upper trace). ■ $Li_xNi_{1-x}O_2$.

minor residues peaks centered at $2\theta = 37.51$, 43.62, and 63.42° that can be attributed to $Li_xNi_{1-x}O_2$.[8a] This is a common impurity in the synthesis of $LiNi_{0.5}Mn_{1.5}O_4$ when the Ni content x in the $LiNi_xMn_{2-x}O_4$ spinel exceeds 0.2.

The morphology and microstructure of the products were examined by field-emission scanning electron microscope (FESEM). The low-magnification FESEM image (Figure 3a) reveals that the product is composed of uniform microspheres with diameters of 3.5–4.5 μm. It is interesting to observe that a

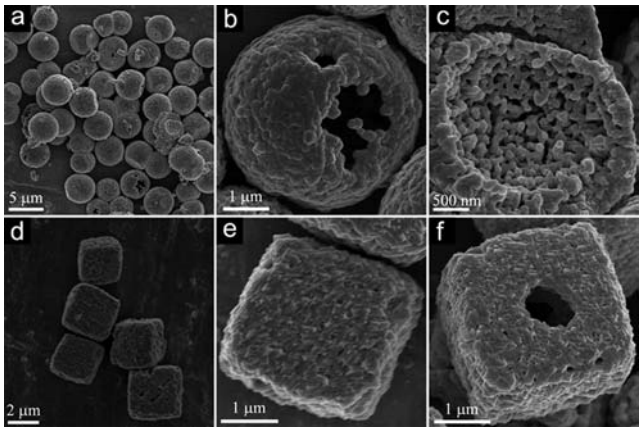

Figure 3. FESEM images of $LiNi_{0.5}Mn_{1.5}O_4$ a)–c) hollow microspheres and d)–f) hollow microcubes.

significant fraction of the microspheres have cracks on their surface. A typical broken hollow microsphere is shown in Figure 3b; the hollow interior can be clearly observed from the broken part. From a broken hemisphere as shown in Figure 3c, it is revealed that the wall of the $LiNi_{0.5}Mn_{1.5}O_4$ hollow microsphere is highly porous and composed of nano-sized/submicrometer-sized subunits. The wall thickness of the hollow microspheres is determined to be about 500 nm. The chemical composition of the products has been analyzed by energy-dispersive X-ray spectroscopy (EDX) (Supporting Information, Figure S5), which confirms an atomic Mn/Ni ratio of 3.0. The use of the pre-grown $MnCO_3$ as the precursor allows for the shape control of the resultant $LiNi_{0.5}Mn_{1.5}O_4$ hollow structures. For example, uniform and well-defined $LiNi_{0.5}Mn_{1.5}O_4$ hollow microcubes with sizes of 3–3.5 μm (Figure 3d) can be obtained by replacing the $MnCO_3$ microspheres with microcubes. The $LiNi_{0.5}Mn_{1.5}O_4$ microcubes have a rough surface (Figure 3e). From the broken part of a $LiNi_{0.5}Mn_{1.5}O_4$ microcube, the hollow interior can be identified unambiguously (Figure 3f).

The electrochemical properties of the $LiNi_{0.5}Mn_{1.5}O_4$ hollow structures were initially investigated by cyclic voltammetry (CV). The first five consecutive CV curves are shown in the Supporting Information, Figure S6. The CV curves for the first two cycles differs significantly from those for the following cycles, and no significant alteration in the CV behavior is observed from the third cycle onwards. From these stabilized CV curves, two pairs of redox peaks associated with the Ni^{2+}/Ni^{3+} and Ni^{3+}/Ni^{4+} couples can be observed in the high-voltage region of 4.60–4.85 V. A pair of minor peaks owing to the Mn^{3+}/Mn^{4+} couple can also be observed at about 4 V. In stoichiometric $LiNi_{0.5}Mn_{1.5}O_4$, which has an ordered spinel structure, the oxidation state of Mn is +4. However, some oxygen deficiency appears during the high temperature calcination, and this reduces a small fraction of Mn^{4+} to Mn^{3+}.

To evaluate the rate capability, the $LiNi_{0.5}Mn_{1.5}O_4$ hollow microspheres were cycled at various charge/discharge rates ranging from 0.1 to 20 C over a potential window of 3.5–5.0 V. A rate of nC corresponds to full charge/discharge of the theoretical capacity in $1/n$ hour, and 1 C is 147 mA h g^{-1} for $LiNi_{0.5}Mn_{1.5}O_4$. For $n > 1$, the constant current charge step is followed by an additional constant voltage charge step till the current drops to $n/10$ C; that is, the cells are first charged at nC to 5.0 V, after 5.0 V is reached, the potential is kept at 5.0 V until the current decreases to one tenth of its initial value. Typical charge and discharge profiles are shown in Figure 4a. In good agreement with the CV results, the discharge curves have a dominant plateau at about 4.7 V and a minor plateau at about 4.0 V. With increasing current density, the discharge capacity only decreases slightly, indicating the excellent rate capability. For the charge curves, the voltage step only contributes a relatively small fraction (ca. 10%) to the total charge capacity. The cycling performance at various rates is shown in Figure 4b. Strikingly, the discharge capacity (118 mA h g^{-1}) at 1C is even larger than that at lower current densities (0.1, 0.2, and 0.5 C). A similar phenomenon has been reported by Lazarraga et al.[10] As the current density increases from 1 to 2, 5, 10, and 20 C, the discharge capacity decreases slightly from 118 to 117, 115, 111.5, and 104 mA h g^{-1}, respectively. After the high rate measurement, the current density is reduced back to 5 C, and a discharge capacity of about 116 mA h g^{-1} can be recovered. The cycling performance of the $LiNi_{0.5}Mn_{1.5}O_4$ hollow microspheres at 1, 2 and 5 C are shown in Figure 4c. Stable cycling performance was obtained for all three rates. For example, after 200 cycles at 2 C, 96.6% of the initial capacity can be retained. The cycling performance of $LiNi_{0.5}Mn_{1.5}O_4$ hollow microcubes was also investigated (Supporting Information, Figure S7). It delivers a discharge capacity of 124 mA h g^{-1} at 2 C, which only decreases slightly to 121 mA h g^{-1} after 200 charge/discharge cycles, corresponding to 97.6% of its initial capacity. When compared to state-of-art $LiNi_{0.5}Mn_{1.5}O_4$

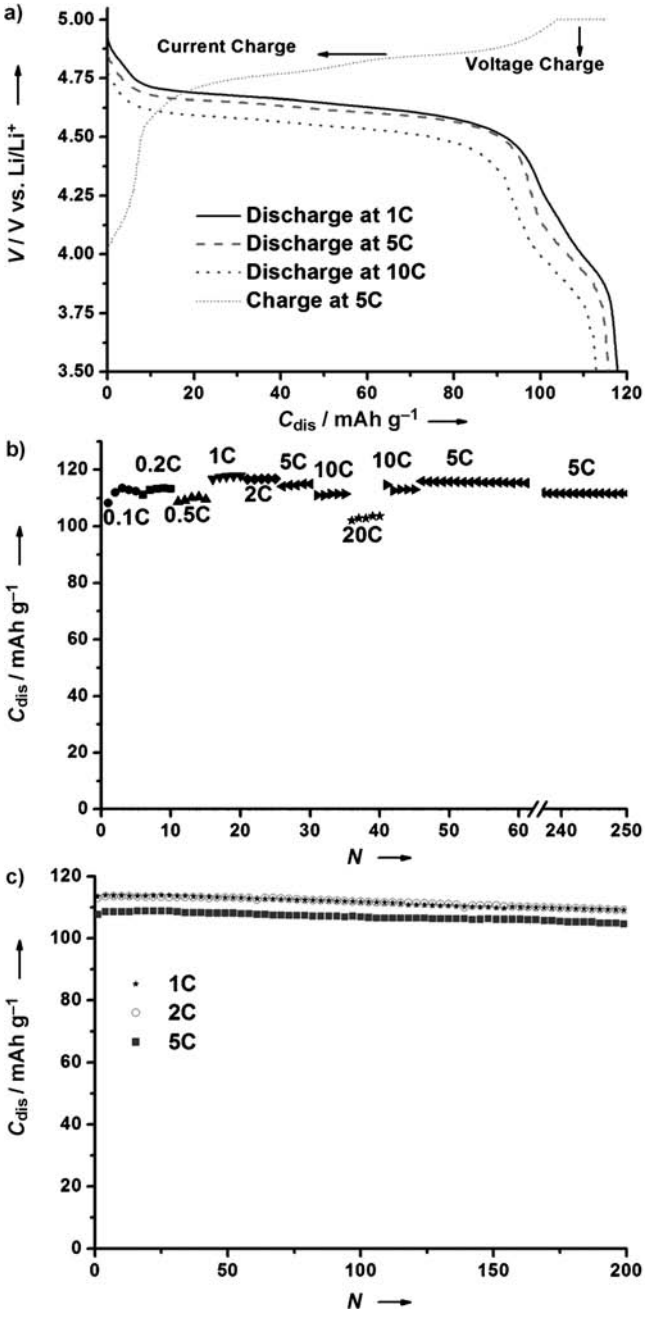

Figure 4. a) Charge/discharge profiles at 1 C, 5 C, and 10 C between 3.5–5.0 V; b) cycling performance at various rates (0.1 C–20 C); c) cycling performance at 1 C, 2 C, and 5 C for 200 cycles. C_{dis} = discharge capacity; N = cycle number.

materials in literature,[8b] it was found that our material exhibits a slightly lower capacity, but better rate and cycling performances.

The excellent rate capability and cycling stability of these $LiNi_{0.5}Mn_{1.5}O_4$ materials might be attributed to the unique nano/micro hierarchical structure. Specifically, the nanosized/submicrometer-sized building blocks provide short distances for Li^+ diffusion and large electrode–electrolyte contact area for high Li^+ flux across the interface, leading to better rate capability. Second, the structural strain and volume change associated with the repeated Li^+ insertion/extraction processes could be buffered effectively by the porosity in the wall and interior void space, thus improving the cycling stability. Finally, the Ni substitution increases the average oxidation state of Mn from 3.5 for $LiMn_2O_4$ to about 4 for $LiNi_{0.5}Mn_{1.5}O_4$, thus effectively suppress capacity fading caused by Mn dissolution and Jahn–Teller distortion.

In summary, uniform $LiNi_{0.5}Mn_{1.5}O_4$ hollow microspheres/microcubes with nanosized building blocks have been synthesized by a facile impregnation approach. The resultant $LiNi_{0.5}Mn_{1.5}O_4$ hollow structures deliver a discharge capacity of about 120 mA h g^{-1} with excellent cycling stability. They also exhibit exceptional rate capability up to 20 C. The superior electrochemical performance suggests the use of these $LiNi_{0.5}Mn_{1.5}O_4$ hollow structures as cathode materials for high-power lithium-ion batteries. The synthesis strategy demonstrated herein is simple and versatile for the fabrication of other metal-doped $LiMn_2O_4$ cathode materials.

Received: October 4, 2011
Published online: November 17, 2011

Keywords: cathodes · hollow structures · lithium-ion batteries · nanostructures · solid-state structures

[1] a) J. M. Tarascon, M. Armand, *Nature* **2001**, *414*, 359 – 367; b) M. Armand, J. M. Tarascon, *Nature* **2008**, *451*, 652 – 657; c) A. S. Aricò, P. Bruce, B. Scrosati, J. M. Tarascon, W. Van Schalkwijk, *Nat. Mater.* **2005**, *4*, 366 – 377.

[2] a) P. G. Bruce, B. Scrosati, J. M. Tarascon, *Angew. Chem.* **2008**, *120*, 2972 – 2989; *Angew. Chem. Int. Ed.* **2008**, *47*, 2930 – 2946; b) Y. G. Guo, J. S. Hu, L. J. Wan, *Adv. Mater.* **2008**, *20*, 2878 – 2887; c) J. S. Chen, L. A. Archer, X. W. Lou, *J. Mater. Chem.* **2011**, *21*, 9912 – 9924.

[3] K. M. Shaju, P. G. Bruce, *Chem. Mater.* **2008**, *20*, 5557 – 5562.

[4] a) E. Hosono, T. Kudo, I. Honma, H. Matsuda, H. S. Zhou, *Nano Lett.* **2009**, *9*, 1045 – 1051; b) D. K. Kim, P. Muralidharan, H. W. Lee, R. Ruffo, Y. Yang, C. K. Chan, H. Peng, R. A. Huggins, Y. Cui, *Nano Lett.* **2008**, *8*, 3948 – 3952; c) H. W. Lee, P. Muralidharan, R. Ruffo, C. M. Mari, Y. Cui, D. K. Kim, *Nano Lett.* **2010**, *10*, 3852 – 3856.

[5] Y. L. Ding, J. A. Xie, G. S. Cao, T. J. Zhu, H. M. Yu, X. B. Zhao, *Adv. Funct. Mater.* **2011**, *21*, 348 – 355.

[6] a) J. Y. Luo, L. Cheng, Y. Y. Xia, *Electrochem. Commun.* **2007**, *9*, 1404 – 1409; b) X. L. Xiao, J. Lu, Y. D. Li, *Nano Res.* **2010**, *3*, 733 – 737; c) Y. L. Ding, X. B. Zhao, J. Xie, G. S. Cao, T. J. Zhu, H. M. Yu, C. Y. Sun, *J. Mater. Chem.* **2011**, *21*, 9475 – 9479.

[7] a) J. Y. Luo, Y. G. Wang, H. M. Xiong, Y. Y. Xia, *Chem. Mater.* **2007**, *19*, 4791 – 4795; b) F. Jiao, J. L. Bao, A. H. Hill, P. G. Bruce, *Angew. Chem.* **2008**, *120*, 9857 – 9862; *Angew. Chem. Int. Ed.* **2008**, *47*, 9711 – 9716; c) D. Tonti, M. J. Torralvo, E. Enciso, I. Sobrados, J. Sanz, *Chem. Mater.* **2008**, *20*, 4783 – 4790.

[8] a) Q. M. Zhong, A. Bonakdarpour, M. J. Zhang, Y. Gao, J. R. Dahn, *J. Electrochem. Soc.* **1997**, *144*, 205 – 213; b) J. Hassoun, K. S. Lee, Y. K. Sun, B. Scrosati, *J. Am. Chem. Soc.* **2011**, *133*, 3139 – 3143; c) J. C. Arrebola, A. Caballero, M. Cruz, L. Hernan, J. Morales, E. R. Castellon, *Adv. Funct. Mater.* **2006**, *16*, 1904 – 1912; d) K. M. Shaju, P. G. Bruce, *Dalton Trans.* **2008**, 5471 – 5475.

[9] X. W. Lou, L. A. Archer, Z. C. Yang, *Adv. Mater.* **2008**, *20*, 3987 – 4019.

[10] M. G. Lazarraga, L. Pascual, H. Gadjov, D. Kovacheva, K. Petrov, J. M. Amarilla, R. M. Rojas, M. A. Martin-Luengo, J. M. Rojo, *J. Mater. Chem.* **2004**, *14*, 1640 – 1647.

